An Implicit TVD Scheme with $k - L_\epsilon$ Turbulence Model for Computation of Transonic Aerofoil Flows

A. Sedaghat

The Manchester School of Engineering
Aerospace Engineering Division, Oxford Road
Manchester M13 9PL
UK

Abstract

A fast and robust algorithm utilizing an upwind implicit Total Variation Diminishing (TVD) scheme[1] with conjunction of $k - L_\epsilon$ turbulence model has been used to study turbulent transonic flows around aerofoils. A hyperbolic C-mesh has been used to generate an orthogonal grid around aerofoil section which is mostly desirable for turbulent computations.

The numerical results obtained for the RAE 2822 aerofoil are compared with experimental data and other numerical results. Contrast to a relatively coarse mesh is used, the quality of the numerical results is very good compared with the other numerical results.

1. Introduction

The TVD concept first proposed by Harten[2,3] and then modified and generalized by Yee[4,5,6] who had implemented to solve the two-dimensional Euler equations of gas-dynamics for aerofoil problems. In most of Yee's papers inviscid aerofoil flows have been considered and the main interest is in general flow features such as shock capturing. However, in our study we aim to make the scheme a practical tool for computation of transonic flows over aerofoils and examine the ability of the scheme to accurately predict aerodynamic coefficients. The aerodynamic coefficients which are important from practical point of view can not be resolved efficiently by the original Yee's scheme because of many involved control parameters such as type of limiters, local time-stepping, and dissipation correction at boundaries. Therefore, some modification of the original scheme is introduced[7,8] to obtain more accurate results.

In the present study, the finite-difference explicit part of flux computation in the Yee's implicit scheme has been replaced by a cell-vertex finite-volume scheme and the implicit part and TVD dissipation functions are also modified. Since at steady-state, the solution of implicit schemes converge to explicit part by vanishing the implicit part, we can claim that the final results are truely based on a finite-volume scheme which is mostly desirable for aerofoil flows. The derivation of this class of TVD schemes in two-dimensional generalized curvilinear coordinates and details of the scheme can be found in references [9,10,11] for solving compressible flows. Details of the $k - L_\epsilon$ turbulence model in non-dimensional form used here is explained and the numerical implementation of this turbulent model is discussed.

The goal is to assess the performance of this scheme in terms of numerical accuracy, robustness and convergence rate for transonic aerofoil flows. The RAE 2822 aerofoil is selected as a test case due to a widely experimental datas available for this aerofoil. Furthermore, this aerofoil has been highly used to examine performance of different numerical schemes by many authors.

2. Governing Equations

The nondimensional form of the compressible Navier-Stokes equations in the general curvilinear coordinates in two dimension can be written as

$$\frac{\partial \hat{\mathbf{U}}}{\partial t} + \frac{\partial \hat{\mathbf{F}}}{\partial \xi} + \frac{\partial \hat{\mathbf{G}}}{\partial \eta} = 0 \qquad (1)$$

where

$$\begin{aligned} \hat{\mathbf{U}} &= \mathbf{U}/J \\ \hat{\mathbf{F}} &= (\xi_x \mathbf{F} + \xi_y \mathbf{G})/J \quad , \quad \hat{\mathbf{G}} = (\eta_x \mathbf{F} + \eta_y \mathbf{G})/J \\ J &= \xi_x \eta_y - \xi_y \eta_x \end{aligned} \qquad (2)$$

$\xi = \xi(x, y), \eta = \eta(x, y)$ are coordinate transformation functions and J is the Jacobian of the transformation. The vectors $\mathbf{U}$, $\mathbf{F}$, and $\mathbf{G}$ are given by

$$\mathbf{U} = \begin{bmatrix} \rho \\ \rho u \\ \rho v \\ e \end{bmatrix}$$

$$\mathbf{F} = \begin{bmatrix} \rho u \\ p + \rho u^2 - \tau_{xx} \\ \rho u v - \tau_{xy} \\ (e+p)u - u\tau_{xx} - v\tau_{xy} + q_x \end{bmatrix}$$

$$\mathbf{G} = \begin{bmatrix} \rho v \\ \rho u v - \tau_{xy} \\ p + \rho v^2 - \tau_{yy} \\ (e+p)v - u\tau_{xy} - v\tau_{yy} + q_y \end{bmatrix} \quad (3)$$

where ρ, u, v, p and e are the density, velocity components along the $x\_$ and $y\_$ directions, static pressure and total energy respectively. The components of the shear-stress tensor and the heat flux vector in non-dimensional form are given by

$$\begin{aligned} \tau_{xx} &= \frac{\mu}{Re}\left(\frac{4}{3}\frac{\partial u}{\partial x} - \frac{2}{3}\frac{\partial v}{\partial y}\right) \\ \tau_{yy} &= \frac{\mu}{Re}\left(\frac{4}{3}\frac{\partial v}{\partial y} - \frac{2}{3}\frac{\partial u}{\partial x}\right) \\ \tau_{xx} &= \frac{\mu}{Re}\left(\frac{\partial u}{\partial y} + \frac{\partial v}{\partial x}\right) \\ q_x &= \frac{-\mu\ \gamma}{(\gamma-1)\ Re\ Pr}\frac{\partial (p/\rho)}{\partial x} \\ q_y &= \frac{-\mu\ \gamma}{(\gamma-1)\ Re\ Pr}\frac{\partial (p/\rho)}{\partial y} \end{aligned} \quad (4)$$

where μ, γ, Pr and Re are the dynamic viscosity, ratio of specific heats, the Prandtl number, and the Reynolds number based on the chord length.

The following non-dimensionalization are used to write the governing fluid flow equations, and all subsequent equations, are in non-dimensional form. All dimensional quantities are presented with superscript $*$.

$$x = \frac{x^*}{c^*} \quad , \quad y = \frac{y^*}{c^*} \quad , \quad u = \frac{u^*}{U^*_\infty} \quad , \quad v = \frac{v^*}{U^*_\infty}$$

$$\rho = \frac{\rho^*}{\rho^*_\infty} \quad , \quad T = \frac{T^*}{T^*_\infty} \quad , \quad p = \frac{p^*/p^*_\infty}{\gamma M^2_\infty} \quad , \quad t = \frac{t^*}{c^*/U^*_\infty}$$

$$\mu_l = \frac{\mu^*_l}{\mu^*_{\infty_l}} \quad , \quad \mu_t = \frac{\mu^*_t}{\mu^*_{\infty_l}} \quad , \quad \tau_w = \frac{\tau^*_w}{\rho^*_\infty\ {U^*_\infty}^2}$$

where the freestream quantities are presented with subscript ∞. Here, c^* is chord length, t^* is time, T^* is temperature, μ^*_l is the molecular or laminar viscosity coefficient, μ^*_t is the eddy or turbulence viscosity coefficient and τ^*_w is the wall shear stress. M_∞ is the freestream Mach number.

3. The Numerical Algorithm

The Alternative Direction Implicit (ADI) form of Linearized Conservative Implicit (LCI) TVD scheme in generalized curvilinear coordinates can be written as[6,11]

$$\begin{aligned} \{\mathbf{I} + \Delta t_{ij}\ (\mathbf{H}^\xi_{i+1/2,j} - \mathbf{H}^\xi_{i-1/2,j})\}\frac{\mathbf{E}^*}{J} &= \frac{\mathbf{RHS}}{J} \\ \{\mathbf{I} + \Delta t_{ij}\ (\mathbf{H}^\eta_{i,j+1/2} - \mathbf{H}^\eta_{i,j-1/2})\}\frac{\mathbf{E}^n}{J} &= \frac{\mathbf{E}^*}{J} \end{aligned} \quad (5)$$

with $\mathbf{U}^{n+1} = \mathbf{U}^n + \mathbf{E}^n$. The operatores $\mathbf{H}^\xi$ and $\mathbf{H}^\eta$ are defined as

$$\begin{aligned} \mathbf{H}^\xi_{i\pm1/2,j}\mathbf{E}^* &= \frac{1}{2}[\hat{\mathbf{A}}_{i\pm1,j}\mathbf{E}^*_{i\pm1,j} - \mathbf{\Omega}^\xi_{i\pm1/2,j}\mathbf{E}^*] \\ \mathbf{H}^\eta_{i,j\pm1/2}\mathbf{E}^n &= \frac{1}{2}[\hat{\mathbf{B}}_{i,j\pm1}\mathbf{E}^n_{i,j\pm1} - \mathbf{\Omega}^\eta_{i,j\pm1/2}\mathbf{E}^n] \end{aligned} \quad (6)$$

The Jacobian matrices $\hat{\mathbf{A}}$ and $\hat{\mathbf{B}}$ result from the linearization of the flux vectors $\hat{\mathbf{F}}$ and $\hat{\mathbf{G}}$ respectively. For steady-state applications

$$\begin{aligned} \mathbf{\Omega}^\xi_{i+1/2,j}\mathbf{E}^* &= M^\xi_{i+1/2,j}\mathbf{I}(\mathbf{E}^*_{i+1,j} - \mathbf{E}^*_{i,j}) \\ \mathbf{\Omega}^\eta_{i,j+1/2}\mathbf{E}^n &= M^\eta_{i,j+1/2}\mathbf{I}(\mathbf{E}^n_{i,j+1} - \mathbf{E}^n_{i,j}) \end{aligned} \quad (7)$$

The scalar values M^ξ and M^η are

$$\begin{aligned} M^\xi_{i+1/2,j} &= \max[\psi(a^l_{i+1/2})] \\ M^\eta_{i,j+1/2} &= \max[\psi(a^l_{j+1/2})] \end{aligned} \quad (8)$$

where I is the 4×4 identity matrix, ψ is called entropy correction function and is given in Equation (12). $a^l_{i+1/2}$ and $a^l_{j+1/2}$ are the eigenvalues corresponding to the Jacobian matrices $\hat{\mathbf{A}}$ and $\hat{\mathbf{B}}$, respectively. The quantities with superscript l throughout this text present arrays with 4 elements, $l = 1, 2, 3, 4$. The **RHS** here is a combination of a cell-vertex finite-volume[12] approach and the numerical dissipation of the Yee's TVD scheme as:

$$\begin{aligned} \mathbf{RHS} &= -\frac{\Delta t_{i,j}}{A_{i,j}}\sum_{AB}^{DA}(\mathbf{F}\Delta y - \mathbf{G}\Delta x) \\ &- \frac{\Delta t_{i,j}}{2}[(\mathbf{R}_{i+1/2,j}\mathbf{\Phi}_{i+1/2,j} - \mathbf{R}_{i-1/2,j}\mathbf{\Phi}_{i-1/2,j}) \\ &+ (\mathbf{R}_{i,j+1/2}\mathbf{\Phi}_{i,j+1/2} - \mathbf{R}_{i,j-1/2}\mathbf{\Phi}_{i,j-1/2})] \end{aligned} \quad (9)$$

The elements of array $\Phi_{i+1/2}$ denoted by $(\phi^l_{i+1/2})^U$ for the second-order upwind TVD scheme[9,10], are given by

$$\begin{aligned} (\phi^l_{i+1/2})^U &= \frac{1}{2}\psi(a^l_{i+1/2})(g^l_{i+1} + g^l_i) \\ &- \psi(a^l_{i+1/2} + \gamma^l_{i+1/2})\alpha^l_{i+1/2} \end{aligned} \quad (10)$$

with the functions γ and ψ defined as

$$\gamma^l_{i+1/2} = \frac{1}{2}\psi(a^l_{i+1/2})\begin{cases} (g^l_{i+1} - g^l_i)/\alpha^l_{i+1/2} & \alpha^l_{i+1/2} \neq 0 \\ 0 & \alpha^l_{i+1/2} = 0 \end{cases} \quad (11)$$

$$\psi(z) = \begin{cases} |z| & |z| \geq \epsilon \\ (z^2 + \epsilon^2)/2\epsilon & |z| < \epsilon \end{cases} \quad (12)$$

with $\epsilon = 0.125$. The characteristic function $\alpha^l_{i+1/2}$ is defined as

$$\alpha^l_{i+1/2} = \mathbf{R}^{-1}_{i+1/2}(\mathbf{U}_{i+1} - \mathbf{U}_i) \quad (13)$$

with $\mathbf{R}$ is right eigen-vector matrix.
In all test cases, the Van-Leer limiter functions $g^l_{i+1/2}$ is used and is given by[1,9]

$$\begin{aligned} g^l_i &= \{\alpha^l_{i-1/2}[(\alpha^l_{i+1/2})^2+\delta]+\alpha^l_{i+1/2}[(\alpha^l_{i-1/2})^2+\delta]\} \\ &\quad /[(\alpha^l_{i+1/2})^2+(\alpha^l_{i-1/2})^2+2\delta] \end{aligned} \tag{14}$$

with δ a small parameter ($10^{-7} \le \delta \le 10^{-5}$). In all the above equations the Roe's averaging[13] is used to evaluate $\mathbf{U}_{i+1/2}$ and corresponding terms.

4. $k - L_\epsilon$ Turbulence Model

The present one-equation turbulence model is very similar to that adopted by Jhonston[14]. A modelled transport equation for the turbulent kinetic energy k is solved in conjunction with the mean-flow equations. Turbulent length scales, required to close the turbulence model, are defined in algebraic form. In fact, experience to date with two-equation turbulence models does not indicate any significant improvement in predictive capability for transonic aerofoil flows[15].

The modelled k transport equation is given by:

$$\frac{\partial W_t}{\partial t}+\frac{\partial F_t}{\partial x}+\frac{\partial G_t}{\partial y}=S_t \tag{15}$$

where $W_t = \rho k$ is containing conserved variables and the fluxes can be divided in convective and diffusive parts

$$F_t = F_t^I + F_t^V \qquad G_t = G_t^I + G_t^V \tag{16}$$

where

$$\begin{aligned} F_t^I &= \rho u k \qquad F_t^V = \beta_{kx}/Re_\infty \\ G_t^I &= \rho v k \qquad G_t^V = \beta_{ky}/Re_\infty \end{aligned} \tag{17}$$

where the viscous diffusion terms are modelled by assuming a simple scalar gradient diffusion process as follows

$$\beta_{kx} = \left(\mu+\frac{\mu_t}{\sigma_k}\right)\frac{\partial k}{\partial x} \qquad \beta_{ky} = \left(\mu+\frac{\mu_t}{\sigma_k}\right)\frac{\partial k}{\partial y} \tag{18}$$

The source term S_t in Equation (15) contains production terms P_k, together with the rate of turbulent kinetic energy dissipation ϵ as follows

$$S_t = P_k - \rho\epsilon \tag{19}$$

where P_k, consists of three parts,

$$P_k = P_{k1} + P_{k2} + P_{k3} \tag{20}$$

where

$$\begin{aligned} P_{k1} &= \frac{\mu_t}{Re_\infty}\left[2\left(\left[\frac{\partial u}{\partial x}\right]^2+\left[\frac{\partial v}{\partial y}\right]^2\right)+\left(\frac{\partial u}{\partial y}+\frac{\partial v}{\partial x}\right)^2\right] \\ P_{k2} &= -\frac{\mu_t}{Re_\infty}\frac{2}{3}\left(\frac{\partial u}{\partial x}+\frac{\partial v}{\partial y}\right)^2 \\ P_{k3} &= -\frac{2}{3}\rho k\left(\frac{\partial u}{\partial x}+\frac{\partial v}{\partial y}\right) \end{aligned} \tag{21}$$

In Equation (20), P_{k1} and P_{k2} are positive and negetive generation, respectively, while P_{k3} can be positive and negetive depending on the flow subject to expansion or compression. In order to distinguish the positive and negetive parts of the source term S_t in the numerical procedure, the following relation has been used

$$S_t = S_t^+ + S_t^- \tag{22}$$

where

$$\begin{aligned} S_t^+ &= P_{k1} + \max(P_{k3}, 0) \\ S_t^- &= P_{k2} + \min(P_{k3}, 0) - \rho\epsilon \end{aligned} \tag{23}$$

The eddy-viscosity relation used in conjunction with the transport equation of k is

$$\mu_t = Re_\infty C_\mu \rho k^{1/2} L_\mu \tag{24}$$

The rate of dissipation of k is modelled via a dissipation length scale L_ϵ and is given by

$$\epsilon = \frac{k^{3/2}}{L_\epsilon + \delta} \tag{25}$$

where δ is a very small number, e.g. 10^{-30}, to avoid division by zero. The two length scales L_μ and L_ϵ are defined by algebraic relations, their formulation being in two parts for the wall boundary layer. In the inner region, the length scales vary linearly with distance from the wall, modified by damping functions in the molecular viscosity dominated region immediately adjacent to the surface.

$$\begin{aligned} L_{\mu i} &= C_1 y_n\left[1-\exp\left(-\frac{R_k}{A_\mu}\right)\right] \\ L_{\epsilon i} &= C_1 y_n\left[1-\exp\left(-\frac{R_k}{2C_1}\right)\right] \end{aligned} \tag{26}$$

where R_k is a Reynolds number characteristic of the turbulence

$$R_k = Re_\infty \rho k^{1/2} y_n/\mu_l \tag{27}$$

Both length scales are taken to be constant in the outer region.

$$L_{\mu o} = L_{\epsilon o} = y_{max} \tag{28}$$

Blending functions are used to ensure a smooth matching of the inner and outer formulations

$$\begin{aligned} L_{\mu i} &= L_{\mu o}\tanh(L_{\mu i}/L_{\mu o}) \\ L_{\epsilon i} &= L_{\epsilon o}\tanh(L_{\epsilon i}/L_{\epsilon o}) \end{aligned} \tag{29}$$

y_{max} is the maximum value of the normal distance from wall y_n at which the following damping function $F(y_n)$ becomes exterma.

$$F(y_n) = [1-\exp(-y^+/A^+)]\ y_n\ |\omega| \tag{30}$$

where ω is the vorticity

$$\omega = \frac{\partial u}{\partial y} - \frac{\partial v}{\partial x} \tag{31}$$

and y^+ is determined from

$$y^+ = \frac{Re_\infty y}{\mu_{lw}}\sqrt{\rho_w \tau_w} \tag{32}$$

where μ_{lw} is the molecular viscosity at wall and τ_w is the shear stress at wall

$$\tau_w = \frac{\mu_w}{Re_\infty}\left(\frac{\partial U_T}{\partial y}\right)_w \tag{33}$$

where U_T is the mean-velocity component tangential to the surface.

The one-equation model involves six constants

$$\sigma_k = 1 \qquad C_\mu = 0.09 \qquad k = 0.418$$
$$A_\mu = 76 \qquad A^+ = 26 \qquad C_1 = \frac{k}{C_\mu^{0.75}} = 2.5$$

4.1 Numerical Implementation

In order to solve the k equation numerically similar finite-difference approach is used in this study. Therefore, it is firstly needed to write the k equation in general coordinate system as follows

$$\frac{\partial \hat{W}_t}{\partial t} + \frac{\partial \hat{F}_t}{\partial x} + \frac{\partial \hat{G}_t}{\partial y} = \hat{S}_t \tag{34}$$

where

$$\hat{W}_t = \frac{1}{J}W_t \qquad \hat{F}_t = \frac{1}{J}(\xi_x F_t + \xi_y G_t)$$
$$\hat{S}_t = \frac{1}{J}S_t \qquad \hat{G}_t = \frac{1}{J}(\eta_x F_t + \eta_y G_t) \tag{35}$$

This equation is approximated by a second-ordered central-difference discretization as below

$$\hat{W}_t^{n+1} - \hat{W}_t^n = R\hat{H}S = -\frac{\Delta t}{2\Delta\xi}(\hat{F}_{t\,i+1,j} - \hat{F}_{t\,i-1,j})$$
$$-\frac{\Delta t}{2\Delta\eta}(\hat{G}_{t\,i,j+1} - \hat{G}_{t\,i,j-1}) + \Delta t S_t \tag{36}$$

The following under-relaxation technique is used to achieve a smooth converged solution.

$$\hat{W}_t^{n+1} = \hat{W}_t^n + \alpha R\hat{H}S \tag{37}$$

The value of the under-relaxation parameter α is in the range of $0 < \alpha < 1$.
During an iterative process, ϵ may grow to ∞ at some mesh points in high gradient regions and putting ϵ in S_t will lead to a negetive k at the next itteration. Therefore, the following linearization is used for the source term to ensure the positiveness of the turbulence kinitic energy k wherever is required. This is given by

$$S_t = S_t^+ + S_t^- W_t^{n+1} \tag{38}$$

Thus, the positive part of the source term is kept at right-hand-side while the negetive part is moved to the other side in Equation (36).

5. Results and Discussion

Results are presented in this section of calculation of the RAE 2822 covering a range of conditions from fully subcritical flow to supercritical flow with shock-induced separation. The calculations are made using the method with a fixed set of flow algorithm and grid generation parameters.

Computational grids are constructed using the algebraic grid generator of Rizzi[16] together with a hyperbolic grid generator of Alsalihi[17] to produce an orthogonal C-mesh for the test cases (see Fig. 1). A relatively coarse mesh of 141×61 has been used in order to investigate performance of the numerical results. The outer boundary is placed at 18 chord lengths away from the aerofoil surface. The first cell-size at both the leading edge and the trailing edge is fixed to $\frac{\Delta\xi}{c} = 0.002$ and $\frac{\Delta\eta}{c} = 0.00002$. In the wake region 24×61 grid points have been placed between the upper and the lower wake cut and the outflow boundary which is placed 10 chords length downstream of the trailing edge.

Each test case was initialized with a uniform freestream flow at the prescribed Mach number and angle of attack. The no-slip condition together with zero normal pressure gradient and normal temperature gradient (adiabatic wall) have been applied on the aerofoil surface. The characteristic boundary condition[18] has been used for the outer-boundary and zero-extrapolation was used for the outflow boundary. In the wake region simple averaging has been applied to all conservative variables.

A local time-stepping similar to Pulliam and Steger[6] is used. This is based on mesh Jacobians as follows

$$\Delta t_{i,j} = \frac{T}{1 + \sqrt{J_{i,j}}} \tag{39}$$

where T is a constant to provide the maximum allowed time-step which can maintain the stability of the numerical scheme. A typical value used in our computation for T is 0.3.

The RAE 2822 aerofoil has been designed for transonic flows and has a maximum thickness/chord ratio of 12.1 % and a sharp trailing edge. An extensive experimental study of this aerofoil in the 8ft $\times$ 6ft transonic wind tunnel at RAE Farnborough was presented by Cook et al[19]. It has been used extensively to validate numerical methods[15].

Figure 1 shows the RAE 2822 aerofoil with a close-up of the computational grid used in the present calculation. Four cases are considered here and the relevant flow conditions are given in Table 1(a). Comparisons of predicted and measured lift, drag and pitching moment

TABLE 1
RAE 2822 Aerofoil
Results using $k - L_\epsilon$ turbulence model
(a) Flow conditions

Case	M	α	$R_e \times 10^{-6}$
1	0.676	1.93^o	5.7
6	0.725	2.54^o	6.5
9	0.730	2.79^o	6.5
10	0.750	2.81^o	6.2

b) Comparison of measured and calculated loads

Case 1	C_L	C_D	$C_M(1/4)$
Experiment	0.566	0.0085	-0.082
Johnston $(k - L_\epsilon)$	0.5799	0.01067	-0.08752
present $(k - L_\epsilon)$	0.5944	0.0087	-0.08811

Case 6	C_L	C_D	$C_M(1/4)$
Experiment	0.743	0.0127	-0.095
Johnston $(k - L_\epsilon)$	0.7446	0.01500	-0.09145
present $(k - L_\epsilon)$	0.8037	0.01324	-0.09734

Case 9	C_L	C_D	$C_M(1/4)$
Experiment	0.803	0.0168	-0.099
Johnston $(k - L_\epsilon)$	0.7909	0.01869	-0.09407
present $(k - L_\epsilon)$	0.8589	0.01809	-0.10272

Case 10	C_L	C_D	$C_M(1/4)$
Experiment	0.743	0.0242	-0.106
Johnston $(k - L_\epsilon)$	0.7910	0.02836	-0.1095
present $(k - L_\epsilon)$	0.8157	0.02957	-0.1157

coefficients and also Johnston's[14] numerical results are shown in Table 1(b), the results being presented for the $k - L_\epsilon$ turbulence model. Note that Johnston's results are based on a fairly fine mesh consisting of 272 $\times$ 64 cells.

Transition is fixed at 11 % chord for Case 1 and at 3 % chord for the others on the upper and lower surfaces of the aerofoil.

Considering the Case 1 which involves mainly subcritical flow, the agreement with measurements is fairly good, especially, drag prediction is very close to experiment. Figure 2 shows that pressure coefficient on upper and lower aerofoil surfaces are fairly matched with results from experiment. The predicted skin friction is generally in good agreement with measurements. Drag convergence is oscillatory due to the relatively large time step is used. However, convergence can be achieved in around 3000 iterations for engineering applications.

Case 6 presents a supercritical flow on the upper surface terminated by a shock wave of moderate strength just downstream of the mid-chord position. Drag and moment coefficients predicted by present method are in good agreement with measurements. However, the predicted lift coefficient is a little higher than the other numerical scheme and measurement. This may be improved by reducing the outer boundary distance from surface. As shown in Figure 3, the shock wave position is slightly mismatch with measured values. Relatively good agreement in skin friction is achieved downstream of the shock wave, but, relatively poor prediction is observed upstream of the shock wave which results from the discrepancies between predicted and measured pressure coefficient at leading edge. This can be resulted from coarseness of mesh points particularly at the leading edge. Rapid and robust convergence of drag coefficient is found.

The drag and moment coefficients are matched better with the measurements for Case 9. In Figure 4, the shock wave position is slightly far downstream. The upper surface skin friction distribution, in Figure 4(b), indicates no separation at the foot of the shock wave for the $k - L_\epsilon$ turbulent model. No separation in the experiment is reported for this case[15]. However, some turbulence models predict a seperation at the foot of the shock wave. Similar convergence with the other test cases is observed.

Case 10 is the most interesting of the RAE 2822 cases to be considered, since it is the only one in which shock-induced separation is present in the experiment. Figure 5 shows that there are now larger discrepancies between prediction and measurements. A small separation is obtained using $k - L_\epsilon$ turbulence model at the foot of shock wave. Convergence is achieved after 6000 itteration. In fact, this turbulence model is very sensetive for separated flows and it is more likely to predict unsteady results.

6. Conclusion

In the initial phase of this study, a fast algorithm utilizing an upwind, implicit, Total Variation Diminishing (TVD) scheme has been developed. Turbulent transonic flows over aerofoils have been studied. A hyperbolic C-mesh has been used to provide an orthogonal grid around the aerofoil section. This study has shown that aerodynamic coefficients can be predicted fairly accurately using a relatively coarse orthogonal grid. The current study of transonic flows has indicated that drag reduction techniques such as passive-shock-control can also be investigated by such a method and any possible drag reduction can be analyzed in detail. This is the subject of current research.

References

[1] Yee, H. C., Warming R. F. and Harten A., "Implicit Total Variation Diminishing (TVD) Schemes for Steady-State Calculations", *J. Comp. Phys.*, 57, pp.

327-360, 1985.
[2] Harten A., "On a Class of High Resolution Total-Variation Stable Finite-Difference Schemes," *NYU Report*, Oct. 1982; *SIAM J. Num. Analysis*, Vol. 21, pp. 1-23, 1983.
[3] Harten A., "A High Resolution Scheme for the Computation of Weak Solutions of Hyperbolic Conservation Laws," *J. Comp. Phys.* , 49, pp. 357-393, 1983.
[4] Yee, H. C. and Harten A., "Implicit TVD Schemes for Hyperbolic Conservation Laws in Curvilinear Coordinates," *AIAA J.*, Vol. 25, No. 2, pp. 226-274, 1986.
[5] Yee, H. C., "Numerical Experiments with a Symmetric High-Resolution Shock- Capturing Scheme," *Procceding of Tenth International Conference on Numerical Methods in Fluid Dynamics*, Lecture Notes in Physics 264, Beijing, China, 1986.
[6] Yee, H. C., "Linearized Form of Implicit TVD Schemes for the Multidimensional Euler and Navier-Stokes Equations," *Advances in Hyperbolic Partial Differential Equations, International Journal on Computers and Mathematics with Applications*, Vol. 12 A, Nos. 4/5, pp. 413-432, 1986.
[7] Sedaghat, A., Shahpar, S. and Hall, I.M.,"Mixed Finite-Difference Finite-Volume TVD Scheme ", *International Conference on Finite-Volume Schemes in Complex Problems*, Rouen, France, July 1996.
[8] Sedaghat, A., Shahpar, S. and Hall, I.M.,"Drag Reduction for Supercritical Aerofoils," *20th ICAS Congress*, Sorrento, Italy, 8-13 September 1996.
[9] Sedaghat, A, "Comparative Study of High-Resolution Shock-Capturing Schemes for External Supersonic Flows", *MSc thesis*, Manchester University, 1993.
[10] Montagne, J. L. and Yee, H. C., "Comparative Study of High-Resolution Shock-Capturing Schemes for a Real Gas," *AIAA J.*, Vol. 27, No. 10, pp. 1332-1346, 1988.
[11] Yee, H. C., Klopfer, G. H. and Montagne, J. L. "High-Resolution Shock-Capturing Schemes for Inviscid and Viscous Hypersonic Flows," *NASA TM-100097*, April 1988.
[12] Fletcher, C. A. J., "Computational Techniques for Fluid Dynamics," *Springer-Verlag*, 1988.
[13] Roe, P. L., "Approximate Riemann Solvers, Parameter Vectors, and Difference Schemes," *J. Comp. Phys.*, Vol. 43, pp. 357-372, 1981.
[14] Johnston, L. J., "Solution of the Reynolds-Averaged Navier-Stokes Equations for Transonic Aerofoil Flows," *Aeronautical J.*, pp. 253-273, 1991.
[15] Holst, T. L., "Viscous Transonic Airfoil Workshop Compendium of Results ," *AIAA Paper No. 87-1460*, 1987; *J. Aircraft*, Vol. 25, No. 12, pp. 1073-1087, 1988.
[16] Rizzi, A. and Vivand H., "Numerical Methods for the Computation of of Inviscid Transonic Flows with Shock Waves," *Notes on Numerical Fluid Mechanics* , Vol 3, Vieweg, 1981.
[17] Alsalihi, Z., "Two Dimensional Hyperbolic Grid Generation," *Von Karman Institute for Fluid Dynamics, Technical Note 162*, October 1987.
[18] Jameson, A. and Baker, T. J., "Solution of the Euler Equations for Complex Configurations," *AIAA Paper No. 83-1929*, 1983.
[19] Cook, P. H., McDonald, M. A., and Firmin, M. C. P., "Aerofoil RAE 2822 - Pressure Distribution, and Boundary Layer and Wake Measurements", *AGARD AR 138*, Paper A6, May 1979.

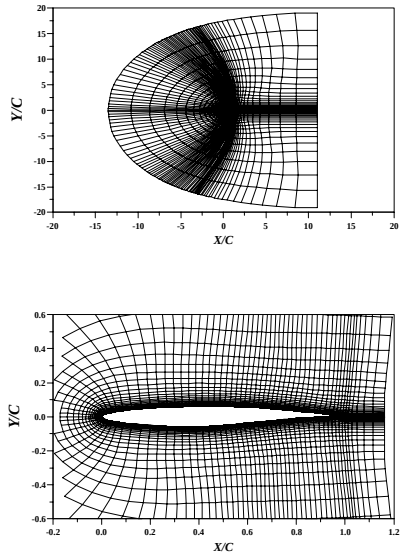

Figure 1: A global and sectional view of the C-hyperbolic mesh generated around the RAE 2822 aerofoli.

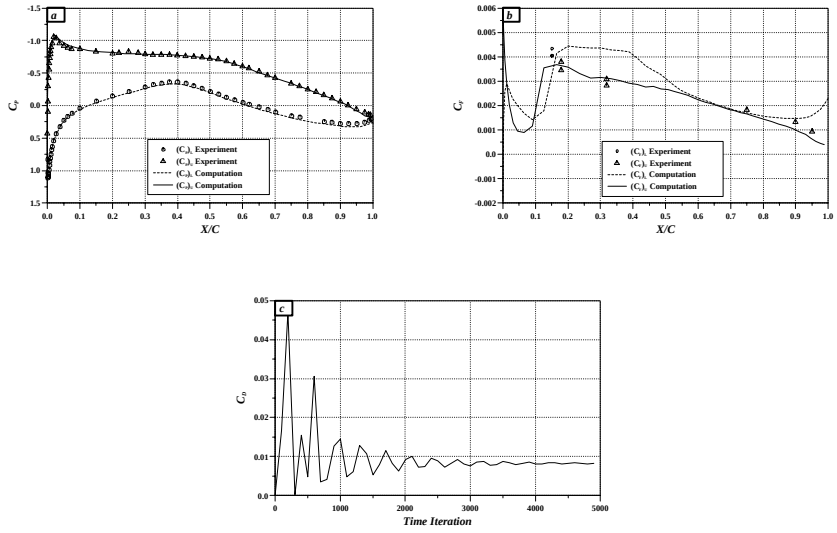

Figure 2: Results for the RAE 2822 aerofoil (case 1), $M = 0.676$, $\alpha = 1.93^o$, $Re = 5.7 \times 10^6$. a) surface pressure coefficient, b)surface skin friction coefficient, c) drag convergence, and d) pressure contours.

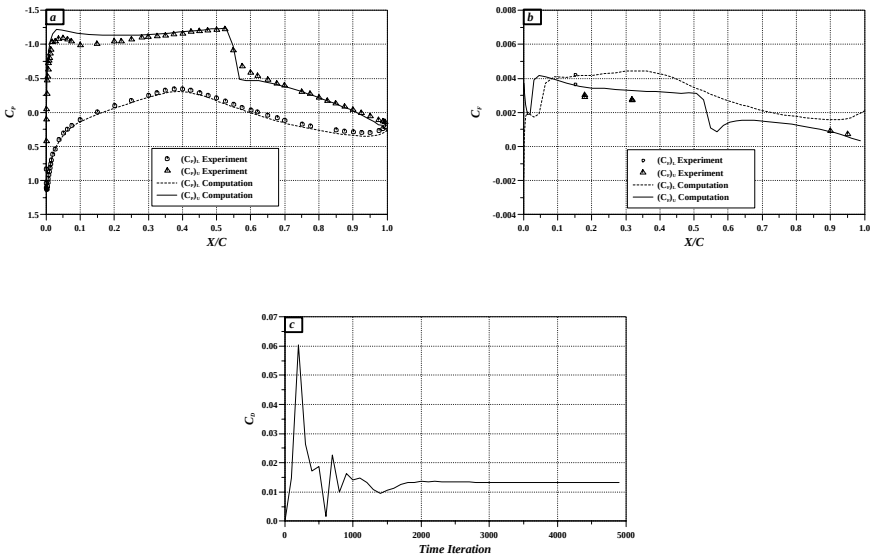

Figure 3: Results for the RAE 2822 aerofoil (case 6), $M = 0.725$, $\alpha = 2.54^o$, $Re = 6.5 \times 10^6$. a) surface pressure coefficient, b)surface skin friction coefficient, c) drag convergence, and d) pressure contours.

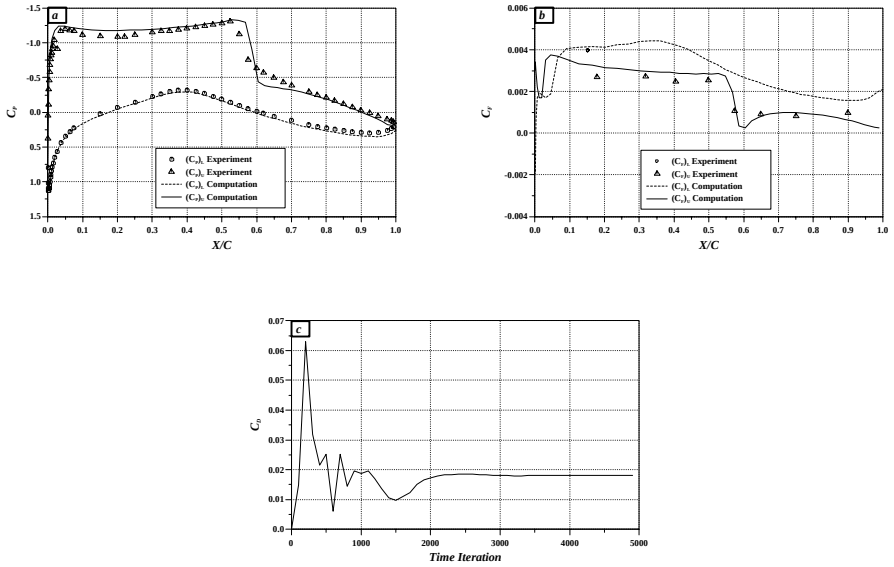

Figure 4: Results for the RAE 2822 aerofoil (case 9), $M = 0.73$, $\alpha = 2.79^o$, $Re = 6.5 \times 10^6$. a) surface pressure coefficient, b)surface skin friction coefficient, c) drag convergence, and d) pressure contours.

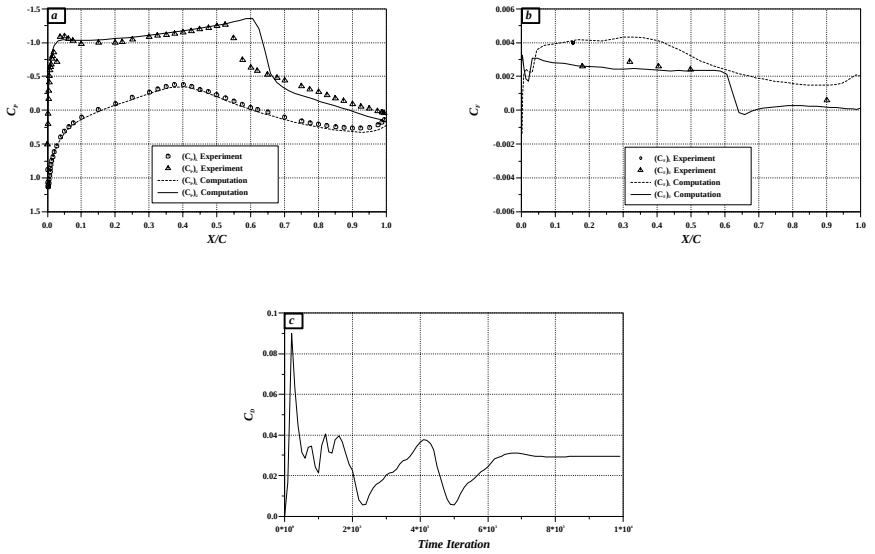

Figure 5: Results for the RAE 2822 aerofoil (case 10), $M = 0.75$, $\alpha = 2.81^o$, $Re = 6.2 \times 10^6$. a) surface pressure coefficient, b)surface skin friction coefficient, c) drag convergence, and d) pressure contours.